48th AIAA Aerospace Sciences Meeting Including the New Horizons Forum and Aerospace Exposition
4 - 7 January 2010, Orlando, Florida

AIAA 2010-1210

Mars Entry, Descent, and Landing Trajectory and Atmosphere Reconstruction

Soumyo Dutta* and Robert D. Braun.†
Georgia Institute of Technology, Atlanta, GA 30332-0150

Flight data from an entry, descent, and landing (EDL) sequence can be used to reconstruct the vehicle's trajectory as well as compute the associated uncertainty. The atmospheric profile encountered by the vehicle can also be estimated from flight data. Past Mars missions have contained instruments, such as accelerometers, gyroscopes, and radar altimeters that do not provide direct measurement of the free-stream atmospheric conditions. Thus, uncertainties in the atmospheric reconstruction and the aerodynamic database knowledge cannot be separated. However, the upcoming Mars Science Laboratory (MSL) will take measurements of the pressure on the aeroshell forebody during entry. These measurements will provide means to determine the free-stream conditions and to separate the atmospheric and aerodynamic uncertainties. In this paper, analytical methods to statistically determine trajectories and free-stream conditions from flight data and to quantify uncertainties in these estimates are discussed. A sample data set from the ballistic range test of Orion Crew Exploration Vehicle (CEV) is then used to demonstrate results from applying these procedures. This approach utilizes the same techniques and toolset planned for subsequent application for the reconstruction of MSL's EDL sequence in 2012.

Nomenclature

a_{0x}, a_{0y}, a_{0z}	=	sensed acceleration at the center of mass
A	=	Jacobian matrix of the equations of motion
B	=	partial derivative matrix of the equations of motion with respect to the state noise
C_A	=	axial force coefficient
C_p	=	coefficient of pressure
e_0, e_1, e_2, e_3	=	quaternions
e	=	state error vector
g	=	gravitational acceleration
H	=	observation sensitivity matrix
I	=	identity matrix
K	=	Kalman gain
m	=	vehicle mass
M	=	Mach number
p, q, r	=	inertial angular velocity components
P	=	pressure
P	=	state covariance matrix
q	=	dynamic pressure
Q	=	state noise covariance matrix
r	=	position

* Graduate Research Assistant, Daniel Guggenheim School of Aerospace Engineering, AIAA Student Member.
† David and Andrew Lewis Professor of Space Technology, Daniel Guggenheim School of Aerospace Engineering, AIAA Fellow.

$\mathbf{R}$	=	observation error covariance matrix
S	=	vehicle reference area
V	=	planet-centric velocity magnitude
u, v, w	=	planet-centric velocity components
$\mathbf{w}$	=	state noise vector
$\mathbf{x}$	=	state deviation vector
$\mathbf{X}$	=	state vector
$\mathbf{y}$	=	observation residual vector
α	=	angle of attack
β	=	sideslip angle
γ	=	flight path angle
ε	=	observation error
ζ	=	clock angle
η	=	cone angle
θ	=	longitude
Θ	=	pitch angle
ρ	=	density
σ	=	standard deviation
ϕ	=	planet-centric latitude
Φ	=	roll angle
$\mathbf{\Phi}$	=	state transition matrix
Ψ	=	yaw angle

Subscripts and superscripts

b	=	backward pass
f	=	forward pass
i	=	pressure port condition
k	=	time index
t	=	total condition
∞	=	free-stream condition
$\bar{}$	=	nominal value
$\hat{}$	=	best estimate

I. Introduction

POST-FLIGHT reconstruction of the entry, descent, and landing (EDL) sequence has been conducted for every successful Mars mission to provide insight into the vehicle's trajectory and atmospheric conditions encountered during the descent.[1-4] Previous Mars missions have provided flight data from on-board accelerometers, gyroscopes, and radar altimeters, which have allowed estimation of the position, velocity and attitude of the vehicles during the EDL timeline. Moreover, based on the sensed decelerations on the vehicle, the atmospheric profiles encountered by the vehicles have also been estimated.

However, these previous reconstructions[1-4] have used a deterministic process where the uncertainties of the measurements have not been included directly in the estimation. If statistical estimation methods are used to reconstruct the trajectory from flight data, the uncertainties in the observations can be incorporated into the estimation process, yielding the associated uncertainty in the reconstructed data.[5] Moreover, in the past, when the reconstructed trajectory has been used to estimate the atmospheric profile, uncertainties in the atmospheric conditions and in the knowledge of the aerodynamic coefficients of the vehicle have not been separable. As past Mars missions have lacked direct atmospheric measurements and have relied largely on inertial measurements, one could not estimate the free-stream conditions without assuming perfect knowledge of the vehicle aerodynamic database.

The upcoming Mars Science Laboratory (MSL) mission will contain onboard pressure transducers that will measure the pressure along the vehicle forebody.[6] Seven pressure transducers located at known locations on the forebody will capture the pressure distribution on the vehicle through the hypersonic phase of entry. The pressure transducers are part of the Mars Entry, Descent, and Landing Instrumentation (MEDLI) project. One of the project's goals under the Mars Entry Atmospheric Data System (MEADS) program is to determine free-stream conditions such

as dynamic pressure (q_∞) and Mach number (M_∞), and vehicle orientation parameters, such as angle of attack (α) and sideslip angle (β). The pressure transducer measurements will provide surface pressure measurements independent of the inertial measurements and radar altimeter data, thus allowing a reconstruction of atmospheric parameters independent of the aerodynamic uncertainties.

This paper will present a framework on how to use surface pressure measurements in a trajectory and atmosphere reconstruction that integrates the uncertainties in the data within the estimation process. Past work done in trajectory reconstructions using pressure measurements will be presented, and traditional methods of atmospheric estimation will be analyzed. Subsequently, a reconstruction procedure using an extended Kalman filter (EKF) algorithm will be presented to statistically estimate the trajectory. Modifications necessary to incorporate pressure measurements in the process will also be discussed. Finally, data sets from ballistic range test of the Orion Crew Exploration vehicle (CEV) will be used as a test case for the methodology.

II. Deterministic trajectory and atmosphere reconstruction

Traditional reconstruction techniques[1-4] have used deterministic methods to estimate a vehicle's trajectory and atmospheric profile. Data sets have contained acceleration of the center of mass and the Euler angle rates of the vehicle with respect to an inertial reference frame. The acceleration measurements are sensed accelerations (a_{0x}, a_{0y}, and a_{0z}) in the planet-centric coordinate system and the attitude measurements are inertial angular rates (p, q, r) in the vehicle-fixed coordinate system, where x, y, and z-axis refer to North, East, and down directions. To begin the reconstruction, the initial state vector of the vehicle has to also be known. The state vector consists of position, velocity and attitude of the vehicle. Vehicle position is usually in terms of radius from the center of the planet (r), planet-centric latitude (ϕ), and longitude (θ). Planet-detic latitude can replace planet-centric latitude in the state vector, but proper conversion between the two reference frames should be made.[7] Velocity states (u, v and w) are expressed in the vehicle-fixed reference frame. Attitude is usually given in terms of the aerodynamic Euler angles, namely yaw (Ψ), pitch (Θ) and roll angles (Φ). However, the equations of motions involving these angles contain trigonometric functions that approach singularities at certain angle values.[9] In order to avoid this situation, the angles are usually converted into quaternions or Euler parameters (e) that represent attitude of the body using four normalized parameters. The conversion from Euler angles to Euler parameters is given in Eq. (1).

$$e_0 = \cos(\Phi/2)\cos(\Theta/2)\cos(\Psi/2) + \sin(\Phi/2)\sin(\Theta/2)\sin(\Psi/2) \tag{1a}$$

$$e_1 = \sin(\Phi/2)\cos(\Theta/2)\cos(\Psi/2) - \cos(\Phi/2)\sin(\Theta/2)\sin(\Psi/2) \tag{1b}$$

$$e_2 = \cos(\Phi/2)\sin(\Theta/2)\cos(\Psi/2) + \sin(\Phi/2)\cos(\Theta/2)\sin(\Psi/2) \tag{1c}$$

$$e_3 = \cos(\Phi/2)\cos(\Theta/2)\sin(\Psi/2) - \sin(\Phi/2)\sin(\Theta/2)\cos(\Psi/2) \tag{1d}$$

$$e_0^2 + e_1^2 + e_2^2 + e_3^2 = 1 \tag{1e}$$

After expressing the initial states in terms of the state elements discussed above, equations of motion can be used to propagate the trajectory from initial time to final time. Equation (2) displays a set of equations of motion expressed in planet-centric reference frame.[8] The gravitation component of acceleration (g) is dependent on the gravitational model and is usually problem-specific. Normally, a second zonal harmonic model is sufficient for EDL trajectory reconstruction purposes, although higher-fidelity models can be used.

$$\dot{r} = -w \tag{2a}$$

$$\dot{\phi} = u/r \tag{2b}$$

$$\dot{\theta} = v/r\cos\phi - \Omega \tag{2c}$$

$$\dot{u} = a_{0x} + (1/r)(uw - v^2\tan\phi) + g_x \tag{2d}$$

$$\dot{v} = a_{0y} + (1/r)(uv\tan\phi + vw) + g_y \tag{2e}$$

$$\dot{w} = a_{0z} - (1/r)(u^2 + v^2) + g_z \tag{2f}$$

$$\begin{bmatrix} \dot{e}_0 \\ \dot{e}_1 \\ \dot{e}_2 \\ \dot{e}_3 \end{bmatrix} = \frac{1}{2}\begin{bmatrix} -e_1 & -e_2 & -e_3 \\ e_0 & -e_3 & e_2 \\ e_3 & e_0 & -e_1 \\ -e_2 & e_1 & e_0 \end{bmatrix}\begin{bmatrix} p \\ q \\ r \end{bmatrix} \tag{2g}$$

Once the trajectory has been reconstructed, atmospheric parameters can be estimated using the inertial acceleration measurements, knowledge of the aerodynamic coefficients of the vehicle and the velocity history during the descent. Equation (3), which is based on the definition of axial force coefficient (C_A), shows how free-stream

density (ρ_∞) can be estimated from sensed axial acceleration (a_{0x}) and the reconstructed velocity (V). Mass (m) of the vehicle and reference area (S) are also present in the equation.

$$\rho_\infty = \frac{ma_{0x}}{0.5V_\infty{}^2 SC_A} \tag{3}$$

This procedure does not include the uncertainties in the axial force measurements or the aerodynamic coefficients as weighting factors in the estimate of the density. Thus, atmospheric uncertainty and aerodynamic uncertainties are not separable. However, if other measurements, such as pressure transducer data, can be collected during an EDL sequence, the uncertainties in the atmospheric parameters can be quantified independently of the vehicle aerodynamics. This is the motivation behind flight of the MEADS sensors in the upcoming MSL mission.

Observations from on-board pressure transducers to estimate free-stream conditions have been collected previously. The Shuttle Entry Air Data System (SEADS) program of the 1980's used a flush-mounted air data system to estimate the pressure distribution across the Space Shuttle forebody during entry. The MEDLI program's pressure data system is in large part based on the SEADS concept. The SEADS project was able reconstruct the free-stream conditions during shuttle entry successfully, and verified its results with simulation and wind tunnel data.[10] However, reconstructions based on SEADS data did not blend the inertial measurements with the pressure distribution data. Instead, a sequential batch-filter was used together with a database of pressure distributions on the vehicle forebody for different flight conditions to estimate the aerodynamic parameters that would create the pressure measurements at the transducers during an EDL sequence. As such, potential coupling between uncertainties in the trajectory estimate and uncertainties in the atmosphere estimate were not included in the SEADS analysis.

Attempts to reconstruct free-stream conditions for Mars missions in a fashion similar to SEADS have been unsuccessful in the past. The Viking landers, which contained stagnation pressure measurement ports, are the only previous Mars mission to sample atmospheric pressure during the descent. Unfortunately, the pressure data returned from these missions showed significant scatter, limiting application of this dataset.[11] Since the Viking landers, no other successful Mars mission has taken pressure measurements during an EDL sequence. MSL will become the first mission to collect a large volume of Mars pressure data during the hypersonic descent phase. Due to the large uncertainty in our knowledge of the Martian atmosphere, a trajectory reconstruction of a Mars EDL sequence that can also estimate the atmospheric profile with a high degree of certainty would be a significant scientific and engineering resource.

III. Statistical trajectory and atmospheric estimation procedure

Accurate estimation for both the trajectory and atmosphere hinges on a procedure to combine information from the various measurement types into a single estimate of the state. Moreover, the estimate should be biased towards measurement types that are more certain; thus, a weighting factor dependent on the data uncertainty needs to be part of the estimation procedure. There are several estimation algorithms available that allow the use of weighting factors to update an estimate based on the measurements collected. The most common type used in navigation and reconstruction-type applications is the extended Kalman filter. A Kalman filter is based on the idea of creating a nominal trajectory and then predicting values of different types of measurements, such as acceleration, throughout the trajectory. The difference between the actual measurements and the predicted measurements is used to update the nominal trajectory. This statistical estimation procedure is composed of two parts:

i. Measurement equations: A method to predict the measurements at a given state
ii. Statistical filter: An algorithm to combine information from various measurement types

A. Measurement Equations

A key requirement for statistical estimation tools such as the Kalman filter is a representation of what the measurements should be at a given state. The actual measurements can then be compared with the predicted measurements, and the state can be appropriately updated. A Kalman filter is based on linear filter theory, so it assumes the measurements are a linear function of the state vector plus a measurement error. If one considers pressure measurements at n different transducers, the pressure can be expressed as shown in Eq. 4.

$$P_i = f_i(\mathbf{X}) + \varepsilon_i \tag{4a}$$

$$\begin{bmatrix} P_1 \\ \cdot \\ P_n \end{bmatrix} = \begin{bmatrix} f_1(\mathbf{X}) \\ \cdot \\ f_n(\mathbf{X}) \end{bmatrix} + \begin{bmatrix} \varepsilon_1 \\ \cdot \\ \varepsilon_n \end{bmatrix} \tag{4b}$$

Here, P_i is the pressure at the i-th orifice, f represents some function of the state vector (**X**) and ε represents the measurement error. Kalman filter, like many Bayesian statistical estimators, assumes that the measurement error distribution is normal, and the error is an unbiased estimator, i.e. the expectation of the error, E[ε] = 0. For most measurement types, f is a non-linear function, but using a first-order Taylor series expansion, Eq. 4 can be linearized about a point $\overline{\mathbf{X}}$ (the nominal estimate of the state) as shown in Eq. 5, where **x** is the deviation in state from $\overline{\mathbf{X}}$.

$$P_i = f_i(\overline{\mathbf{X}}) + \left[\partial f / \partial \mathbf{X}\right]_{\mathbf{X}=\overline{\mathbf{X}}} \mathbf{x} + \varepsilon_i \tag{5}$$

A measurement sensitivity (Jacobian) matrix (H), as seen in Eq. 6, can now be defined.

$$H \equiv \left[\partial f_1 / \partial \mathbf{X} \quad \cdot \quad \partial f_n / \partial \mathbf{X} \quad \partial f_n / \partial \mathbf{X}\right]^T_{\mathbf{X}=\overline{\mathbf{X}}} \tag{6}$$

The measurement sensitivity equations have to be developed for various measurement types. Christian et al. discusses the development of the sensitivity matrix for accelerometer and radar altimeter measurements.[5] In addition, a special modification of the Kalman filter, known as the Kalman-Schmidt filter, can estimate systematic errors in the measurement types. Measurement sensitivity equations for accelerometer and radar measurements in such cases can be found in Refs. 7 and 12. In the present analysis, pressure data measurement equations and their sensitivity matrices are discussed.

Measurement sensitivity expressions for pressure data are developed by numerical differentiation due to the complexity of the expressions relating the trajectory states with the aerodynamic states. The measurement prediction expressions are functions of the state vector that normally consists of the position, velocity, and attitude of the vehicle. However, for the pressure measurement case, free-stream pressure (p_∞) and free-stream density (ρ_∞) are added to the state vector. Their equations of motion are derived from the hydrostatic equation and an atmospheric equation of state, respectively (Eq. 7). For this study, the isothermal gas equation of state was used, but any other state equation that takes advantage of a model of the gas dynamics can be substituted.

$$\dot{P}_\infty = \rho_\infty g w \tag{7a}$$

$$\dot{\rho}_\infty = \rho_\infty^{\,2} g w / P_\infty \tag{7b}$$

During the hypersonic phase, the velocity of the vehicle is large with respect to the wind velocity. So the planet-relative velocity can be used to calculate the angle of attack and angle of sideslip (Eq. 8). The relative velocity to the wind should be used for more precision. In those cases, the wind speed is included as a part of the state vector, but an equation of motion for the wind speed must then be included. For simplicity, winds are not modeled in this study. The two orientation angles can then be combined into a total angle of attack, α_t (also Eq. 8).

$$\alpha = \tan^{-1}(w/u) \tag{8a}$$

$$\beta = \sin^{-1}(v/V) \tag{8b}$$

$$\alpha_t = \cos^{-1}(\cos\alpha \cos\beta) \tag{8c}$$

The velocity magnitude can be used to calculate the local Mach number. The speed of sound needed for Mach number calculation is a strong function of altitude and can be calculated from the state vector. Finally, the pressure port locations have to be stated. Normally, the locations of these orifices are known in terms of clock (ζ) and cone (η) angles. The cone angle describes the orifice's location with respect to the maximum diameter of the aeroshell. The clock angle describes the port's location on the aeroshell from the y-axis in the y-z plane. Since the pressure ports' orientation with respect to the forebody does not change during the flight, the cone and clock angles are constant throughout the trajectory. Once the total angle of attack, Mach number and the clock and cone angles of the ports are known, the pressure coefficient (C_P) at each orifice can be found from tables created from the vehicle aerodynamic database. An example of such a table is shown in section IV as Table 2. After the pressure coefficient is found, the pressure at each surface location can be calculated using the vehicle velocity and free-stream pressure and density which are state elements. The sensitivity matrix can be calculated by perturbing each of the state elements by a small amount and calculating the change in the predicted port pressure. This numerical method of calculating the sensitivity matrix is necessary since a closed form solution is not possible due to the fact that the pressure coefficient values are being computed from tables. Numerical ill-conditioning issues can arise based on what tolerance value is used to perturb the pressure prediction equations.

B. **Extended Kalman Filter**[13, 14]

The next step in the reconstruction process is to use a statistical filter to combine the measurement information with the nominal estimate of the state. For this study, this process was achieved using an extended Kalman filter. A

Kalman filter is based on linear filter theory and uses the difference between predicted and measured data to update the estimate of the state. An extended Kalman filter is a modification of the original Kalman filter to express the nonlinearity in the system dynamics that is lost in the linearization needed for the original Kalman filter. Consider the linearization of the state vector at time increment k as a function of the state at time k-1 and a random state noise vector (**w**) as seen in Eq. 9. Recall that **x** is the deviation in state and **X** is the state vector.

$$\mathbf{X}_k = \mathbf{X}_{k-1} + \left[\frac{\partial \mathbf{X}(t_k)}{\partial \mathbf{X}(t_{k-1})}\right]\mathbf{x}_{k-1} + \mathbf{w} = \mathbf{X}_k + \Phi_k \mathbf{x}_{k-1} + \mathbf{w} \tag{9}$$

The state transition matrix (**Φ**) is the function that propagates the state from k-1 to k. The linear Kalman filter needs a nominal trajectory from the initial state to the end state, and the filter estimates the deviation in the state around this nominal trajectory. The extended Kalman filter does not need a nominal trajectory from the start to the end of the trajectory. Instead, the propagation from k-1 to k is done using the nonlinear equations of state. Then, when the state estimate is updated at time k using the measurements, this new estimate is used to propagate to time k+1. Thus, the nonlinearity inherent in the system dynamics can be better handled using the extended Kalman filter algorithm rather than the linearized Kalman filter.

In addition to the equation that defines the state vector, relationships are also needed to define the uncertainty in the state and how these values propagate over time. In Eq. 4, ε was introduced as the measurement error. The state vector also has a similar error term known as the state error vector ($\mathbf{e}_k$) which contains the error in each element of the state vector at time k. EKF assumes that the state error is also normally distributed and thus a state covariance matrix (**P**) can be introduced which is defined as $E[\mathbf{e}_k\mathbf{e}_k^T]$. A measurement covariance matrix ($\mathbf{R}_k$) can be defined at time k where $\mathbf{R}_k = E[\varepsilon\varepsilon^T]$.

As is the case with the state vector, the state covariance vector must be propagated from time k-1 to k. State transition matrices can be used to accomplish this operation as seen in Eq. 10, where $\mathbf{Q}_k$ is the state noise covariance (i.e. $\mathbf{Q}_k = E[\mathbf{w}\mathbf{w}^T]$).

$$\mathbf{P}_k = \Phi_{k-1}\mathbf{P}_{k-1}\Phi_{k-1}^T + \mathbf{Q}_{k-1} \tag{10}$$

A Riccatti-type differential equation can also be used to update the covariance vector as seen in Eq. 11. Here **A** is the Jacobian of the equations of motion with respect to the state vector and produces a matrix similar to what is found in Eq. 6 for the measurement expressions. **B** is the partial derivatives of the equations of state with respect to the state noise vector. All of these matrices are evaluated at the current time k-1 and are used to propagate P to time k.

$$\dot{\mathbf{P}} = \mathbf{A}\mathbf{P} + \mathbf{P}^T\mathbf{A}^T + \mathbf{B}\mathbf{Q}\mathbf{B}^T \tag{11}$$

In order to begin the EKF process, a nominal estimate at the current time must be found. If the current time is k, then the nominal state estimate ($\bar{\mathbf{X}}_k$) can be found from the final estimate at k-1 as described before. The covariance matrix can be similarly estimated at time k ($\bar{\mathbf{P}}_k$).Then, the best state estimate at time k ($\hat{\mathbf{X}}_k$) is found by Eq. 12a, where K_k is the Kalman gain (Eq. 12b) and $\mathbf{y}_k$ is the measurement residual vector. The measurement residual vector (**y**) is defined as the difference between all of the actual measurements at the current time and the corresponding predicted measurements at the nominal state. Within the expression for the Kalman gain, H_k is the measurement sensitivity matrix and evaluated at time k. Finally, the state covariance for the best estimate ($\hat{\mathbf{P}}_k$) is found using Eq. 12c. In Eq. 12c, I is the identity matrix.

$$\hat{\mathbf{X}}_k = \bar{\mathbf{X}}_k + K_k\mathbf{y}_k \tag{12a}$$

$$K_k = \bar{\mathbf{P}}_k H_k^T\left(H_k\bar{\mathbf{P}}_k H_k^T + R_k\right)^{-1} \tag{12b}$$

$$\hat{\mathbf{P}}_k = (I - K_k H_k)\bar{\mathbf{P}}_k(I - K_k H_k)^T + K_k R_k K_k^T \tag{12c}$$

The algorithm for this filter can be summarized as follows:

1) Initialize the state vector and the state covariance matrix at time $t_{k-1}=t_0$ and let k =1, where k is an index of the epoch when measurement was taken.
2) Read in measurement at time t_k.
3) Calculate a nominal state at t_k ($\bar{\mathbf{X}}_k$) by integrating the non-linear equations of motions (Eqs. 2 and 7) with $\hat{\mathbf{X}}_{k-1}$ as the initial condition.
4) Calculate the nominal state covariance matrix ($\bar{\mathbf{P}}_k$) using the state transition matrix (Eq. 10) or the Riccati equations (Eq. 11).
5) Calculate the measurement residual vector ($\mathbf{y}_k$), the measurement sensitivity matrix (H_k), and the Kalman gain (K_k) using the nominal state and state covariance (Eq. 12b).

6) Calculate the best estimate of the state ($\hat{\mathbf{X}}_k$) and state covariance ($\hat{\mathbf{P}}_k$) using Eqs. 12a and 12c.

7) Increment counter k and go back to step 2 until measurements at all times have been read.

A difference between the extended Kalman filter and the standard Kalman filter is highlighted in step 3 of the algorithm where the nominal state is calculated by integrating the non-linear equations and the last best estimate is used as the initial condition. In a highly non-linear problem, large deviations could be propagated through this linear approximation. The extended Kalman filter effectively re-linearizes the state estimate at the last best estimate found whenever a new measurement is processed, thus reducing deviations that can result from linearizing a non-linear problem.

An advantage of the extended Kalman filter is that it provides an efficient way to incorporate more than one type of measurement. Each measurement type has a unique measurement sensitivity matrix and observation covariance. Thus, when the filter is processing measurement type A, the appropriate H and R matrices are used with the nominal state error covariance. If measurement type B has to be processed at the next time step, only the H and R matrices will change in the algorithm.

Moreover, one can see that the state is affected by three factors by looking at Eq. 12b for the Kalman gain and Eq. 12a for the state update. The Kalman gain is a function of the current state uncertainty (P_k), the measurement uncertainty (R_k) and the residual between the predicted and actual measurements (**y**). If the state estimate is more certain than the measurements being processed, the filter will be minimally affected by the data. In addition, the filter can "blend" the information from the various data types, and the state estimate will be weighted towards the measurement with the smallest observation error, which can be gleaned from its observation covariance matrix. When two or more data types are being processed sequentially, the state estimate initially may oscillate between the measurements from the differing sources, but the filter quickly uses the weighting information from the R matrices to calculate the blended estimate. Finally, the residual of the measurements can scale the update of the state. If the predicted measurements were very close to the actual measurements, then the state update will be minimal. To demonstrate this concept, Mars Pathfinder reconstruction data is used below. Details about this trajectory reconstruction can be found in Ref. 5, with additional background information in Ref. 2. Figure 1 demonstrates the effect of data blending by showing the estimate of altitude for Mars Pathfinder when the radar altimeter measurements are included with the accelerometer measurements. One way to compare the effect of uncertainty in the estimate is to vary the weighting factor for the measurements being used. As one can see, the altitude estimate initially oscillates between the accelerometer and radar altimeter observations, but finally the EKF moves the estimate towards the less uncertain measurements, which in this case comes from the radar altimeter.

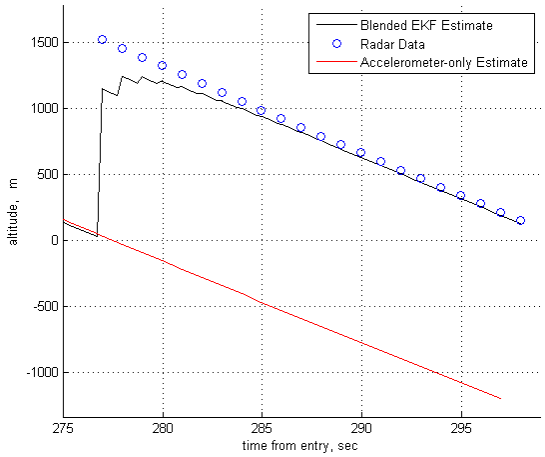

Figure 1: Effect of blending different data types on the estimate of altitude for Mars Pathfinder. The altitude shown is above Mars mean radius.

Another advantage of the extended Kalman filter is that it can be used to sequentially reconstruct the trajectory in either a forward or backwards manner. The reconstruction can be conducted starting from the atmospheric entry all the way down to the ground (forward pass) or using a projected landing location to estimate the trajectory up to the entry conditions (backwards pass). The forward pass starts its estimate from an initial state and covariance that is found independent of the trajectory reconstruction process. Also, the reconstruction is conducted in a chronological manner. The backwards pass has the advantage of starting at a smaller uncertainty value as it begins from the end of

the forward estimate. The forward (f) and backward (b) pass estimates can be combined using the Fraser-Potter smoothing solution,[14] which is shown in Eqs. 13.

$$\hat{\mathbf{P}}_k = \left[\hat{\mathbf{P}}_{fk}^{-1} + \hat{\mathbf{P}}_{bk}^{-1}\right]^{-1} \tag{13a}$$

$$\hat{\mathbf{X}}_k = \hat{\mathbf{P}}_k \left[\hat{\mathbf{P}}_{fk}^{-1}\hat{\mathbf{X}}_{fk} + \hat{\mathbf{P}}_{bk}^{-1}\hat{\mathbf{X}}_{bk}\right] \tag{13b}$$

An advantage of combining both the forward and backward estimates is to find an optimal estimate of the trajectory. The forward pass estimate at time k uses the measurement data from t_{entry} to k, while the backward pass uses the measurement data from time t_{ground} to k. The combined smoothed estimate can use measurement data at all times to create the estimate at k. Figure 2 shows the forward, backward, and smoothed estimate of the altitude of Mars Pathfinder, which is used to demonstrate the advantage of the smoothing algorithm. The one-sigma uncertainties associated with the three estimates are also shown.

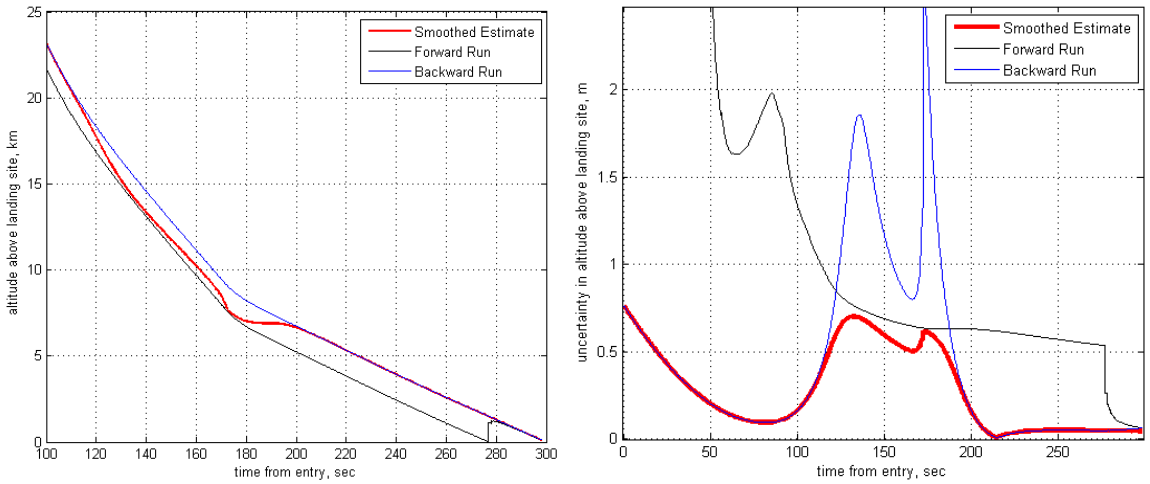

(a) Altitude estimate **(b) 1σ uncertainty in altitude**

Figure 2: Forward and backward runs and smoothing on the estimate of altitude for Mars Pathfinder.

IV. Test Case

Results from a sample case are presented in this section to test the methodology. As MSL will not provide a data set until 2012, measurements from a ballistic range test of a Crew Exploration Vehicle (CEV) model is used to apply the trajectory and atmospheric reconstruction procedures.[16] The ballistic range test was conducted on July 15, 2008 at the Aberdeen Army Proving Ground (APG) in Aberdeen, MD. As shown in Figure 3, the test utilized two titanium models of the CEV. The models were referred to as the pressure-telemetry modules (PTM). The PTMs were launched from a ballistics range gun and data was collected for approximately 20 seconds after they exited the muzzle. Although data sets for both models were available, only the results for the second model (labeled PTM2) are analyzed below. Some key parameters for PTM2 are summarized in

Table **1**. The center of gravity (CG) locations are with respect to U.S. Army Research Laboratory coordinate system convention.

(a) PTM1 **(b) PTM2**

Figure 3. CEV models used in the pressure-telemetry tests.[16]

Table 1. Physical parameters for PTM2

Mass	18.422	lb
CG_x	2.488	in
CG_y	0.002	in
CG_z	0.187	in
I_{xx}	69.144	lb-in^2
I_{yy}	50.978	lb-in^2
I_{zz}	51.322	lb-in^2
Length	4.268	in
Diameter	6.500	in
Data sampling rate	7.940	KHz

As can be surmised from the name of the experiment, the models collected pressure data along with telemetry data during their flight. The telemetry information consisted of sensed accelerations, angular rates and magnetometer measurements. Additionally, a tracking radar calculated the range and range rate of the models with respect to a fixed station. Also, the on-site meteorological station provided temperature, pressure and wind speed information.

There are fundamental differences between MSL and this ballistic range test. The ballistic range model achieves a maximum Mach number of 3.5 during its flight, while MSL is going to achieve speeds several times greater. The PTM only climbs up to 800 meters thus the data set will not contain measurements from the upper atmosphere, which can compare well with the thin atmosphere of Mars. Finally, since the PTM is shot out of a gun, it is acted upon by very high accelerations and angular rates at the beginning of the flight. These accelerations are illustrated in Figure 4.

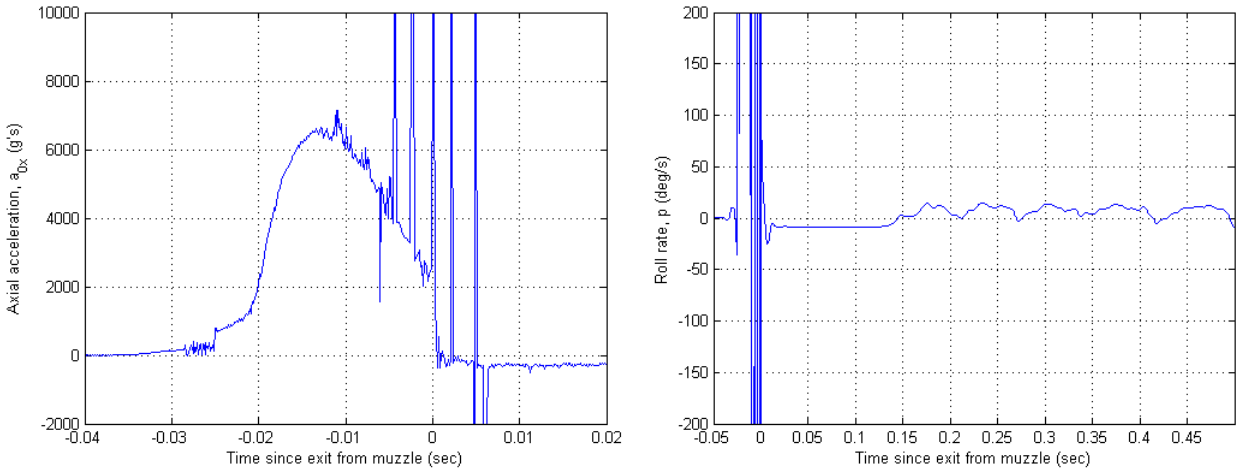

(a) Axial acceleration for PTM2 **(b) Roll rate for PTM2**

Figure 4. Example of inertial measurement unit observations for PTM2.

As one can see from the figure, the vehicle undergoes almost 7000 g's of acceleration and several hundred degrees per second of angular velocity. MSL will not face this type of flight regime. However, despite these differences, the EKF algorithm should be insensitive to the magnitude of data that it handles. Regardless of the actual values of the data, if the measurement equations and the algorithm are simulated correctly and proper values are used for the observation errors, the filter should be able to reconstruct the trajectory and atmosphere that the PTM encounters. Furthermore, since the types of observations that the PTMs obtained are comparable to the types of data MSL is planning to obtain, a successful reconstruction of the PTM's trajectory bodes well for similar success with MSL's data set.

As mentioned in section III, the pressure measurement prediction equations are dependent on tabulated values of the pressure coefficient as function of total angle of attack, Mach number, and the orifice cone and clock angle. An example of such a table for PTM2 is given in Table 2.

Table 2. Pressure coefficient values for PTM2 at M = 0.6 and η = 14 degrees

Angle of attack, α (deg)	Clock Angle, ζ (degrees)					
	0	5	10	15	20	25
0	1.096745	1.096747	1.096749	1.09675	1.096752	1.096754
5	1.096761	1.096763	1.096764	1.096766	1.096768	1.09677
10	1.096772	1.096774	1.096776	1.096778	1.096779	1.096781
15	1.09678	1.096781	1.096783	1.096785	1.096786	1.096788
20	1.096783	1.096784	1.096786	1.096788	1.096789	1.096791
25	1.096781	1.096783	1.096784	1.096786	1.096788	1.096789
30	1.096775	1.096777	1.096778	1.09678	1.096782	1.096783
35	1.096765	1.096767	1.096768	1.09677	1.096771	1.096773
40	1.09675	1.096752	1.096753	1.096755	1.096756	1.096758
45	1.096731	1.096733	1.096734	1.096736	1.096737	1.096739

To match data types with MSL, this analysis only considered the acceleration, angular rates, radar measurements and pressure observations from the PTM2 data set. As was shown in Eq. 2, accelerations and angular rate information are used in the equations of motion to propagate the state one time increment to another. So these measurement types are not explicitly used in the EKF tool using Eq. 12. However, the state noise vector (**v**) is defined based on the measurement error of the accelerometer and gyroscopes, thus the uncertainty in these data appears implicitly in the EKF through the state noise covariance matrix, **Q**. The pressure measurements were taken at five port locations on the forebody of the vehicle. Figure 5 shows the locations of the ports on the forebody of the vehicle and pressure data from those ports during the trajectory. Figure 6 displays the range data from the tracking radar.

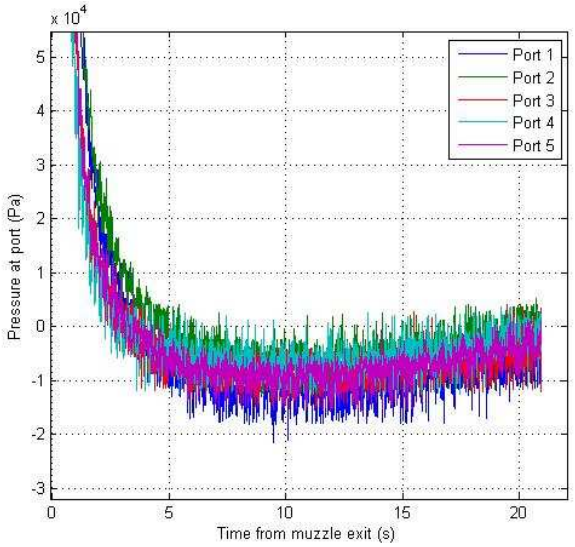

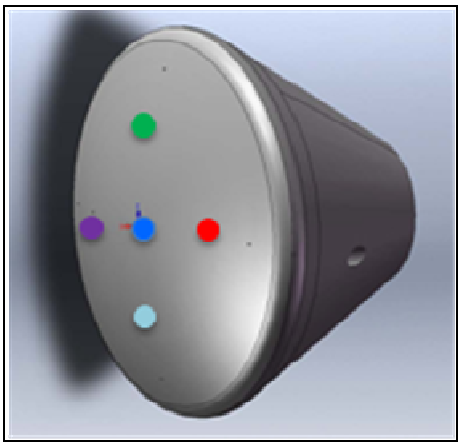

(a) Pressure port observations **(b) Pressure port locations on vehicle forebody[16]**

Figure 5. Pressure port locations and observations for PTM2

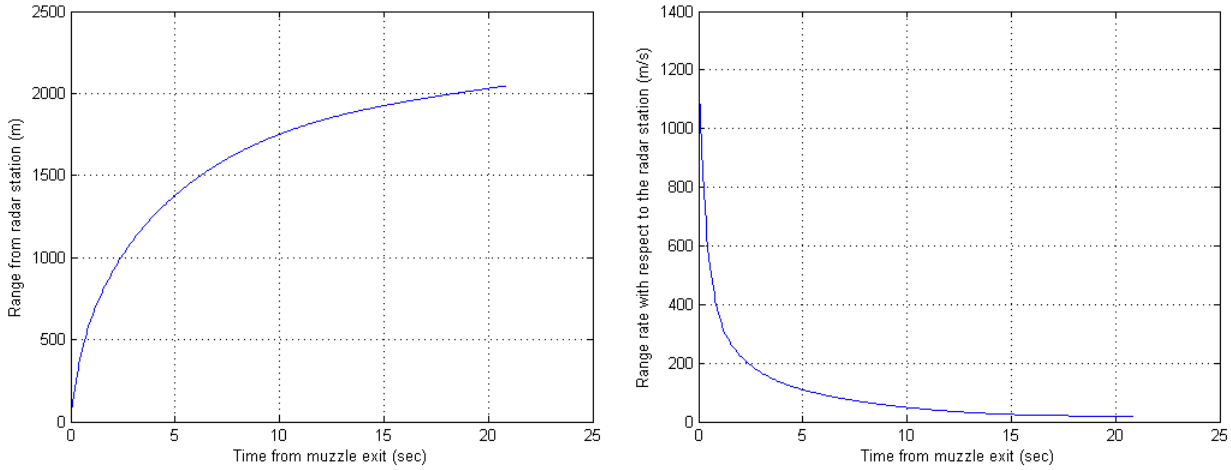

(a) Range from radar station **(b) Range rate relative to the station**

Figure 6. Tracking radar observations for PTM2

The instruments and their measurement errors are summarized in Table 3. The measurements errors reported in the table are the 1σ values and the errors are assumed to be normally distributed with an expectation of zero.

Table 3. Measurement uncertainties of sensors on PTM2

Observation	Sensor Model	1σ uncertainty
Accelerometers	ADXL-78	0.0686 m/s
Angular rates	ADXRS300	0.025 deg/s
Pressure transducers	XCEL-100-500A	5 psi
Radar position	APG tracking radar	
Distance		1 m
Angles		0.1146 deg
Radar rate	APG tracking radar	
Rate		1 m/s
Angular rate		0.1 deg/s

As can be surmised from Fig. 4, the initial state of the vehicle at the muzzle exit was hard to assess due to the high acceleration and angular rates encountered by model in the gun. The initial state inside the gun was known, but since the pressure and radar measurements are only taken once the vehicle exits the gun, the initial state for the EKF had to be that point. Thus, using only the accelerometer and angular rate measurements, the state vector at 0.001 seconds past the muzzle exit is determined. This data serves as the initial state for the EKF and is summarized in Table **4**. However, since the accelerations and angular rates are so high and the sensors reach saturation at several points, very high values are assigned for the initial state uncertainties. As a result, the forward run of the EKF will be initially more sensitive towards the measurements in updating the states. Note that this aspect of analyzing the PTM data is quite different from what would occur with a Mars data set. The initial state for Mars EDL systems are found from the end state of the navigation orbital determination (OD) solutions, which provide the state vector with high accuracy. Thus, for a Mars reconstruction, the EKF will start from a relatively certain initial state.

Table 4. Initial state vector used for PTM2

t_0	0.001 sec
u	-912.628 m/s
v	25.475 m/s
w	-193.985 m/s
Altitude	2.43 m
ϕ	39.466 deg
θ	283.830 deg
Ψ	195.743 deg
Θ	11.485 deg
Φ	-2.387 deg
P_∞	101.783 kPa
ρ_∞	1.1807 kg/m^3

The smoothed best estimate for PTM2's trajectory and the atmosphere it encountered is given below. The altitude history of the model is seen in Figure 7. A one-sigma uncertainty bound is also shown in the figure.

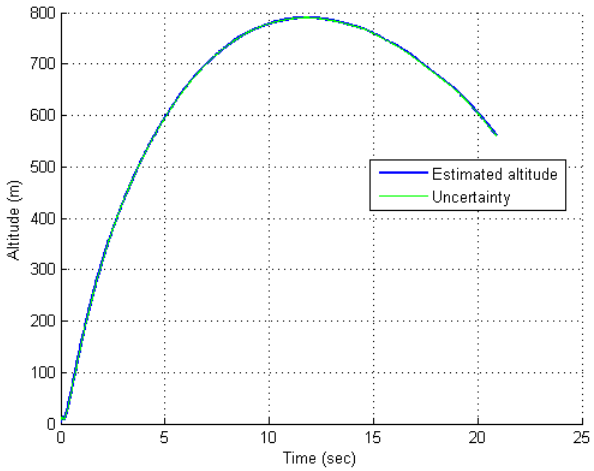

Figure 7. Reconstructed altitude of PTM2 and 1σ uncertainty in the estimate.

The velocity of the model can be seen in Figure 8 in terms of Mach number.

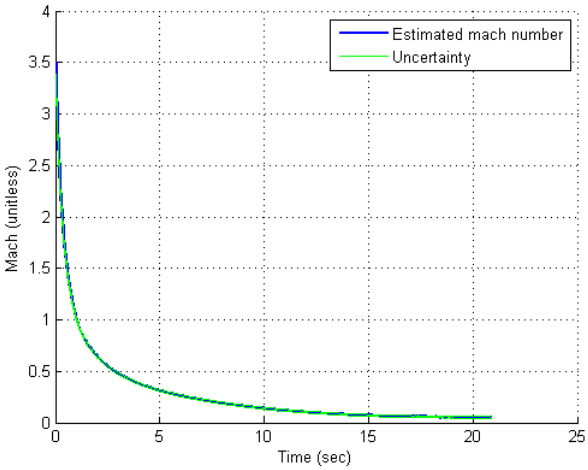

Figure 8. Reconstructed Mach number of PTM2 and 1σ uncertainty in the estimate.

The altitude and Mach number history compare well with simulated results for the test. The figures above also show that the uncertainty in the estimate is small. Although the initial state uncertainties were set to be large numbers, after the forward and backward run and the smoothing procedure, the uncertainty in the state estimates decrease dramatically. Additionally, as was discussed before, the goal of an atmospheric reconstruction is to determine the free-stream pressure and density profile seen by the vehicle during its trajectory. However, since this vehicle only reached about 800 meters, the change in pressure and density was not large. Nevertheless, the reconstructed values for pressure are compared with the data collected by the ballistic range's meteorological station in Table 5. Density data was not given by the meteorological station, and thus it is not shown here. However, the change in density was also just as small as the change in pressure.

Table 5: Reconstructed pressure estimate for PTM2

Altitude (m)	Estimated Pressure (kPa)	±1σ (kPa)	Meteorological Data (kPa)
15	100.122	1.593	101.483
57	99.661	1.691	101.010
112	99.179	1.793	100.377
175	98.607	1.909	99.669
244	98.006	2.044	98.883
322	97.306	2.208	98.011
409	96.484	2.412	97.044
506	95.514	2.671	95.972
615	94.268	5.270	94.785
736	93.058	4.798	93.472

Recall that the meteorological data was not included in the EKF process. The free-stream condition shown above is a result of only inertial measurements, radar measurements and the on-board pressure observations. The fact that it agrees very well with an independent source of pressure observations demonstrates the strength of the reconstruction methodology. Besides free-stream conditions, another objective of MSL's MEDLI program is to determine the orientation angles of the vehicle during entry, descent and landing. As has been shown before, angle of attack and sideslip angle affect the pressure distribution on the vehicle forebody, and thus if these values can be reconstructed, then there will be additional insight towards the vehicle's interaction with the atmosphere. The estimated angle of attack and sideslip angle history for PTM2 are shown in Figure 9.

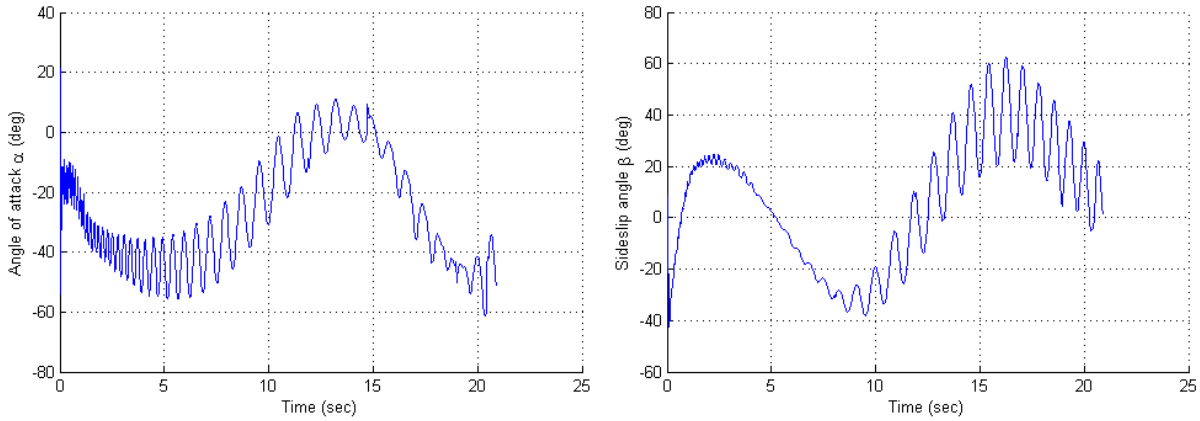

(a) Angle of attack **(b) Sideslip angle**

Figure 9. Reconstructed angle of attack and sideslip angle of PTM2.

Unlike the free-stream pressure estimate there were not any independent observations to compare with the reconstruction of the orientation angles. However, the reconstructed values compared favorably with what was predicted pre-flight. The high accelerations and angular rates experienced by the model (Figure 4) when launched from the gun still have an effect on the reconstruction estimate. The angle of attack and sideslip angles experience significant oscillation in the first one second of flight and this is apparent from looking at the above figures. However,

when the high accelerations dissipate with time, the orientation angles are reconstructed without significant noise. This last observation bodes well for MSL reconstruction as that vehicle will not face the high accelerations and rates seen by PTM2.

V. Conclusion

This paper provides a framework on how to use flight data from an entry, descent, and landing sequence to reconstruct the vehicle's trajectory and atmosphere as well as compute the associated uncertainties in these estimates. Past Mars missions have flown limited instrumentation, such as accelerometers, gyroscopes, and radar altimeters that do not provide measurements directly related to the free-stream conditions. Thus, uncertainties in the atmospheric conditions and aerodynamic database knowledge could not be separated. These previous reconstructions have also relied on a deterministic process where the uncertainties of the measurements were not included directly in the estimation and potential coupling between uncertainties in the trajectory and uncertainties in the atmosphere were not estimated. As the upcoming MSL mission will provide forebody pressure measurements during entry together with accelerometer, gyroscope, and radar altimeter data, the Mars EDL reconstruction process can be significantly improved. In this investigation, a statistical reconstruction procedure based on extended Kalman filter theory was developed to take advantage of this new data type. A sample data set from ballistic range tests of a Crew Exploration Vehicle model was used to show results from applying the methodology. The reconstruction method was able to estimate the states of the CEV model well during its twenty second flight. Moreover, the atmospheric conditions that were reconstructed matched well with the meteorological information and pre-flight predictions. The success of the using the reconstruction methodology on this CEV ground-based test data set demonstrates that the trajectory and atmospheric estimation procedure can be successful in the reconstruction effort for MSL.

VI. Acknowledgments

The authors are grateful to NASA for providing the ballistic range data set used in this analysis. In particular, the primary author is appreciative that he had the opportunity to work at the NASA Langley Research Center (LaRC) and Analytical Mechanics Associates (AMA) during the summer of 2009 and was able to collaborate with Chris Karlgaard of AMA and Mark Schonenberger of LaRC. The paper also utilized an extended Kalman filter tool for trajectory reconstruction created by John Christian at Georgia Institute of Technology. This research was funded by NASA through its Aeronautics Research Mission Directorate Fundamental Aeronautics Program.

References

[1] Euler, E.A., Adams, G.L., and Hopper, F.W., "Design and Reconstruction of the Viking Lander Descent Trajectories," *Journal of Guidance and Control*, Vol. 1, No. 5, Sep-Oct. 1978, pp 372-378.

[2] Spencer, D.A., Blanchard, R.C., Braun, R.D., Kallemeyn, P.H., and Thurman, S.W., "Mars Pathfinder Entry, Descent, and Landing Reconstruction," *Journal of Spacecraft and Rockets*, Vol. 36, No. 3 May-June 1999, pp 357-366.

[3] R.Blanchard, "Entry Descent and Landing Trajectory and Atmosphere Reconstruction for the Mars Exploration Rovers Missions A and B," white paper, performed under NASA-JPL subcontract CCNS20568F, The George Washington University, Washington, D.C., 15 Apr. 2008.

[4] Desai, P.N., Prince, J.L, Queen, E.M., Cruz, J.R., and Grover, M.R., "Entry, Descent, and Landing Performance of the Mars Phoenix Lander," *AIAA/AAS Astrodynamics Specialist Conference and Exhibit*, Honolulu, HI, 18-21Aug. 2008.

[5] Christian, J.A., Verges, A.M., and Braun, R.D., "Statistical Reconstruction of Mars Entry, Descent, and Landing Trajectories and Atmospheric Profiles," *AIAA SPACE Conference and Exposition*, Long Beach, CA, 18-20 Sep. 2007.

[6] Gazarik, M.J., Wright, M.J., Little, A., Cheatwood, F.M., Herath, J.A., Munk, M.M., Novak, J., and Martinez, E.R., "Overview of the MEDLI Project," *IEEE Aerospace Conference*, Big Sky, MT, 1-8 Mar. 2008.

[7] Karlgaard, C.D., Tartabini, P.V., Blanchard, R.C., Kirsch, M., and Toniolo, M.D., "Hyper-X Post-Flight-Trajectory Reconstruction," *Journal of Spacecraft and Rockets*, Vol. 43, No. 1, Jan.-Feb. 2006, pp. 105-115.

[8] Etkin, B., *Dynamics of Atmospheric Flight*, Dover Publications, Inc., Mineola, NY, 2000.

[9] Kuipers, J.B., *Quaternions and Rotation Sequences*, Princeton University Press, Princeton, NJ, 1999, p. 167.

[10] Pruett, C.D., Wolf, H., Heck, M.L., and Siemers, P.M., "Innovative Air Data System for the Space Shuttle Orbiter," *Journal of Spacecraft and Rockets*, Vol. 20, No. 1 Jan-Feb. 1983, pp 61-69.

[11] Ingolbby, R.N., Michel, F.C., Flaherty, T.M., Doty, M.G., Preston, B., Villyard, K.W., and Steele, R.D., "Entry Data Analysis for Viking Landers 1 and 2," NASA CR-159388, Nov. 1976.

[12] Jaswinski, A.H., *Stochastic Processes and Filtering Theory*, Academic Press, San Diego, CA, 1970, pp. 332-347.

[13] Tapley, B.D., Schutz, B.E., and Born, G.H., *Statistical Orbit Determination*, Elsevier Academic Press, Burlington, MA, 2004, Chap. 4.

[14] Zarchan, P., and Musoff, H., *Fundamental of Kalman Filtering, A Practical Approach*, American Institute of Aeronautics and Astronautics, Inc., Reston, VA, 2000.
[15] Fraser, D.C., and Potter, J.E., "The Optimum Linear Smoothers as a Combination of Two Optimum Linear Filters," *IEEE Transactions on Automatic Control*, Vol. 14, No. 8, 1969, pp. 387-390.
[16] Topper, B., "NASA Orion Crew Exploration Vehicle-Pressure Telemetry Module (CEV-PTM) Free Flight Ballistic Range Experiment Performed at APG, MD on July 15, 2008," US Army Research Laboratory internal document, AMSRD-ARL-WM-BA, Aberdeen, MD, 31 July 2008.